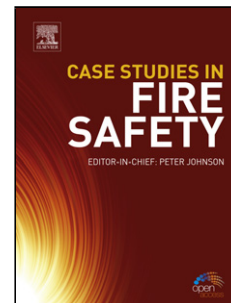# Journal Pre-proof

The role of benzotriazole modified zinc phosphate in preventing corrosion-driven organic coating disbondment on galvanised steel

N. Wint (Validation) (Formal analysis) (Investigation) (Data curation)<ce:contributor-role>Writing - original and draft) (Writing - review and editing) (Visualization) (Supervision), C.M. Griffiths (Validation) (Formal analysis) (Investigation) (Data curation), C.J. Richards (Validation) (Formal analysis) (Investigation) (Data curation)<ce:contributor-role>Writing - original and draft) (Writing - review and editing) (Visualization), G. Williams (Conceptualization) (Methodology) (Writing - review and editing) (Supervision), H.N. McMurray<ce:contributor-role>Conceptualization) (Methodology) (Writing - review and editing) (Supervision)

Please cite this article as: Wint N, Griffiths CM, Richards CJ, Williams G, McMurray HN, The role of benzotriazole modified zinc phosphate in preventing corrosion-driven organic coating disbondment on galvanised steel, *Corrosion Science* (2020), doi: https://doi.org/10.1016/j.corsci.2020.108839

This is a PDF file of an article that has undergone enhancements after acceptance, such as the addition of a cover page and metadata, and formatting for readability, but it is not yet the definitive version of record. This version will undergo additional copyediting, typesetting and review before it is published in its final form, but we are providing this version to give early visibility of the article. Please note that, during the production process, errors may be discovered which could affect the content, and all legal disclaimers that apply to the journal pertain.

The role of benzotriazole modified zinc phosphate in preventing corrosion-driven organic

coating disbondment on galvanised steel

N. Wint [a,*], C. M. Griffiths [a], C.J. Richards [a], G. Williams [a], H. N. McMurray [a]

[a]*Materials Research Centre, College of, Swansea University, Bay Campus, Fabian Way,*

Crymlyn Burrows, Swansea, UK, SA1 8EN

*Corresponding author: E-mail address: n.wint@swansea.ac.uk

Highlights
- Investigation of cathodic delamination of PVB from hot dip galvanized steel.
- Production of corrosion inhibitor whereby BTA adsorbed onto zinc phosphate.
- Comparison of the ability of ZnPhos-BTA and ZnPhos to resist coating delamination.
- pH dependent release of BTA from ZnPhos in presence of NaCl.
- Reduced cathodic delamination rate in presence of ZnPhos-BTA compared to ZnPhos.

Abstract

A simple modification using adsorbed benzotriazole is shown to significantly improve the

performance of zinc phosphate corrosion inhibitive pigment in slowing rates of organic

coating failure. The novel inhibitor, ZnPhos-BTA, is dispersed within a model coating and

the scanning Kelvin probe (SKP) is used to monitor corrosion driven cathodic coating

delamination from hot dip galvanized steel (HDG). Disbondment kinetics are obtained as

a function of pigment volume fraction (ϕ) and compared to those obtained for unmodified

ZnPhos. Additions of 0.1 ϕ ZnPhos-BTA result in an almost 20-fold reduction in delamination rate compared to standard ZnPhos at the equivalent volume fraction.

Keywords: A. Steel, A. Zinc, A. Organic Coatings, C. Atmospheric Corrosion

1. Introduction

Zinc (Zn) based galvanised coatings can provide sacrificial protection to underlying steel substrates and are heavily utilised within the automotive and construction industries, where they are typically used in conjunction with mixed organic/inorganic coating systems [1]. These systems are made up of several layers: a pre-treatment/conversion coating which prepare the substrate and improves the adhesion of the overlying primer, the primer layer which contains corrosion inhibitor pigments, and a topcoat which acts as a barrier to the external environment and is responsible for the aesthetics of the finished product [1]. **Organically coated metal surfaces can fail via a variety of processes including cathodic delamination and filiform corrosion (FFC), which are related to cathodic and anodic blistering respectively [2].** Historically, the ability of organic coatings to resist corrosion driven failure, has relied heavily on the use of dispersed sparingly soluble hexavalent chromium-based pigments. However, Cr(VI) compounds are toxic and carcinogenic, and research is heavily focused on the identification of suitable alternatives [3-14]. Zinc phosphate (ZnPhos) is a well-known corrosion inhibitor pigment which is used extensively within industry as a Cr(VI) replacement and is **associated with a far lower toxicity [15-16].** ZnPhos can be incorporated as part of the pre-treatment and/or as the corrosion inhibitor pigment within the primer layer. In the case of the former, the phosphoric acid used in phosphating baths reacts with metallic Zn to produce an inorganic

$Zn_3(PO_4)_2$. nH_2O layer which acts as a barrier to further anodic metal dissolution [9-10] and improves adhesion of the overlying organic coating [11-14]. Additional ZnPhos may be incorporated in the form of an anti-corrosion pigment (a dispersion of 1-10 μm ZnPhos submicron powder particles) in the primer coating. ZnPhos is sparingly soluble in water [14] and its dissolution will result in the release of Zn^{2+} cations and phosphate anions into any potentially corrosive electrolyte present at a break or defect in the protective coatings. Both Zn^{2+} and phosphate are known to act as corrosion inhibitors [10-11, 17-22]. Phosphate ions can form a protective passive film on the surface [17-18] and the formation of insoluble metal salts can also polarize the surface of the substrate [19-20]. However, the low solubility $(Zn_3(PO_4)_2\ K_{sp} = 9\ x\ 10^{-33}\ mol^5 dm^{-15})$ [23] of ZnPhos means that its effectiveness is limited [7-9, 18-22, 24-27]. The production of inhibitors based on organic-inorganic complexes have been suggested as a promising way to incorporate inhibitors into organic coatings [8].

Small organic molecules (low molecular weight organics) such as benzotriazole (BTA) has been investigated heavily as potential corrosion inhibitors, primarily for zinc, copper and brass [28-39], as well as aluminium [40]. However, it is normally added in solution and is not typically used as a simple solution in a film forming polymer for reasons of migration (into other coating layers). It is therefore advantageous to convert BTA into a solid particulate form (pigment) that is insoluble in the film forming polymer (binder) of the priming paint layer. **A solid and bound form of BTA would also reduce the leachability of the species and limit the environmental concerns associated to it [41-42].** Furthermore, organic inhibitor heteroatoms can react with organic coating functionalities. This process can result in a reduction in cross linking density and loss of inhibitor

properties [7]. The curing process can also result in chemical interference between organic coatings and organic inhibitors that contain hydrogen [8].

The amphoteric nature of BTA means that its form depends on solution pH according to the protonic equilibria given by Equations (1) and (2) [37].

$$BTAH_2^+ \leftrightarrow BTAH + H^+ \qquad \text{(pK}_{a1}\text{=1.1)} \qquad (1)$$

$$BTAH \leftrightarrow BTA^- + H^+ \qquad \text{(pK}_{a2}\text{=8.2)} \qquad (2)$$

The anionic form of BTA (benzotriazolate (BTA^-)) has previously been exchanged into the layered double hydroxide, hydrotalcite, to form a pigment for use in organic coatings applied to aluminium alloys [43-46]. BTA has also been incorporated into mesoporous SiO_2 and polymeric nanocontainers for use with zinc and HDG [47-48] and, more recently, a novel corrosion inhibitor pigment based on benzotriazolium cations ($BTAH_2^+$) exchanged into an ion exchange resin, has proved to be effective in preventing the cathodic delamination of a model PVB coating from a HDG surface [49].

The corrosion behaviour of Zn in BTA containing phosphate solutions has been studied previously [28-29] and BTA has been shown to adsorb onto a ZnPhos covered zinc surface [30]. Elsewhere, BTA has been found to interact with zinc ions to form a $Zn(BTA)_2$ salt [32-36]. Other work has focused on the development of Zn-BTA based corrosion inhibitive pigments [7], as well as (ZnPhos)-BTA [50] and potassium zinc phosphate (PZP)-BTA pigments [8] produced using co-precipitation methods. PZP-BTA pigments provided superior inhibition of steel corrosion than either PZP or ZnPhos. This enhanced performance was attributed to the combination of inorganic (PZP) species, which was believed to retard anodic kinetics, and organic (BTA) species, which reduced cathodic kinetics [8]. Protonated BTA molecules were believed to adsorb on the cathodic sites via

electrostatic attraction. Metal complexes of BTA were also detected. The additional corrosion protection provided was attributed to the nature and morphology of the insoluble film deposited on the steel samples [8].

The aims of the work to be described here are 1.) to evaluate the efficiency of Zn-Phos as a corrosion inhibitive pigment **for the protection of HDG, for which the prevailing mechanism of organic coating failure occurs via cathodic delamination [2],** 2.) to assess whether simple modification of the same industry standard Zn-Phos pigment, using BTA, can produce a significantly effective inhibitor, and 3.) to identify the principal modes by which the novel pigment works to retard cathodic disbondment. In so doing, BTA is adsorbed onto the surface of ZnPhos using a rotary evaporation process. The ZnPhos-BTA pigment is dispersed within an ethanolic solution of polyvinyl butyral co-alcohol co-acetate (PVB), which is then coated onto a HDG surface. **Coating disbondment is initiated from an artificial coating defect in a Stratmann type cell which allows for the accurate identification of the relevant coating failure mechanism.** The delamination process is monitored using a scanning Kelvin probe (SKP) technique [51-53]. By following this well-established methodology, it is possible to complete a systematic study of the effect of ZnPhos-BTA pigment volume fraction (ϕ) on the kinetics of cathodic coating delamination.

2. Materials and Methods

2.1 Materials

Hot dipped galvanised steel (HDG) was supplied by TATA Steel UK and consisted of 0.7 mm gauge, mild steel coated with a 20 μm zinc layer (containing 0.15 wt.% aluminium) on each side. Coupons were cut from a larger sheet and were 5 cm x 5 cm in size. Zinc phosphate PZ20 (> 97 % purity, ~ 4.5 μm diameter), was supplied by Société Nouvelle des

Couleurs Zincique (SNCZ). Polyvinyl butyral-*co*-vinyl alcohol-*co*-vinyl acetate (PVB), molecular weight 70,000-100,000, benzotriazole (> 99 % purity), and all other chemicals, were obtained from Sigma-Aldrich Chemical Company and of analytical grade purity.

2.2 Methods

Pigment preparation; Adsorption of BTA on zinc phosphate

BTA was adsorbed onto ZnPhos using a rotary evaporator. 300 cm^3 of a 10 wt.% ethanolic solution of BTA was prepared in a round bottomed flask. Once the BTA had dissolved, 270 g ZnPhos was added to the mixture such that a 9:1 ratio of ZnPhos to BTA was achieved. Once the ZnPhos had become fully dispersed within the ethanolic mixture, the round bottomed flask was attached to a rotary evaporator and slowly lowered into a water bath maintained at 50°C. The flask was rotated at a constant speed and water was passed through the condensation tube. This allowed the ethanol, contained within the round bottomed flask, to evaporate and condense into the receiving vessel. This process was carried out until formation of a dry white powder occurred. The powder was removed from the flask and dried in an oven at 70°C for 24 hours to drive off any residual moisture. The pigment formed during this process will be referred to as ZnPhos-BTA for the remainder of this paper. The optical appearance of ZnPhos-BTA does not vary significantly from that of ZnPhos; both are white, polydispersed powders.

UV-VIS Spectroscopy;

The release of BTA, from the ZnPhos-BTA pigment, into a series of electrolytes was monitored using a Perkin Elmer Lambda 750 UV/VIS/NIR spectrophotometer. Calibration was completed by plotting the absorbance (*A*) at λ_{max} = 274 nm as a function of BTA$^-$ **concentration** (*c*) for values of concentration between 1 x 10^{-5} mol.dm^{-3} and 1 x 10^{-4}

mol.dm^{-3}. Measurements were taken at 20°C at a pH of 11. Aliquots of the relevant solution were dispensed into 1 cm quartz cuvettes and the absorption spectrum was recorded. A good straight line was obtained indicating that **at pH 11,** aqueous BTA$^-$ (at concentrations between 1 x 10^{-5} mol.dm^{-3} and 1 x 10^{-4} mol.dm^{-3}) obeys Equation 3, (the Beer Lambert law, where ε_{274} is the molar extinction coefficient at 274 nm and l is the optical path length in cm)

$$A_{274} = \varepsilon_{274} cl \tag{3}$$

This indicates that association, precipitation or surface absorption of the BTA$^-$ anions does not occur to a significant degree at these conditions [54]. The value of ε_{274} obtained using Equation 3 was (9700±200) M^{-1}.cm^{-1}. Following calibration, it was possible to monitor the concentration of BTA species present within solutions of varying pH, allowing for determination of the pH dependent nature of BTA release from ZnPhos. 1 g of pigment was dissolved into 1 dm^3 of the chosen electrolyte. The samples were mixed using a magnetic stirrer. After 20 hours a Buchner funnel was used to remove any powder (>1μm) which remained in suspension. Aliquots of solution (10 ml) were withdrawn, diluted to 100 ml using distilled water and, if required, the pH of the solution was adjusted to pH 11 by the drop-wise addition of NaOH (aq). **Each measurement was repeated three times.**

Coating formulation

Pigments were dispersed into the PVB model coating at various volume fractions (ϕ). **Although PVB does not fully represent industrial coating systems it was used in the current work as it allows a measurable degree of delamination over a short time-scale. It is therefore considered to be a suitable alternative when the principal aim is the comparison of materials with respect to their ability to resist corrosion driven coating**

disbondment of organic coatings. The mass of the pigment (M_{pig}) required for each value of ϕ_{pig} was determined using Equation 4, where M_{pol} is the mass of the polymer (0.8 g.cm^{-3}) and ρ_{pig} is the density of the relevant pigment (3.95 g.cm^{-3} for ZnPhos) and ρ_{pol} is the density of the polymer (1.083 g.cm^{-3}).

$$M_{pig} = \frac{\emptyset \times M_{pol} \times \rho_{pig}}{(1-\emptyset) \times \rho_{pol}} \tag{4}$$

An ethanolic slurry of the pigment was made. This was then dispersed in the relevant amount of 15.5 % w/w PVB ethanolic solution using a high shear mixer and the mixture was degassed in an ultrasonic bath.

Cathodic Delamination

The ability of ZnPhos and ZnPhos-BTA to prevent the cathodic driven coating disbondment of PVB from a HDG substrate was investigated using 'Stratmann' [51-52] type corrosion cells. 5 cm x 5 cm sized HDG coupons were cut from larger sheets. An aqueous slurry of 5 μm polishing alumina powder was used to remove any surface oxides and contaminants from the coupons, which were then rinsed with distilled water. Insulating tape was applied to two, parallel sides of each coupon. The tape controlled the thickness of the PVB model coating which was bar cast onto the surface before being allowed to dry in air [53]. The resultant dry PVB film thickness was (30±5) μm, as determined using a micrometer screw gauge. A small area of the bare metal was exposed by partially peeling back the dry coating. This area served as an artificial defect. This defect was separated from the intact polymer coating by a clear adhesive tape/PVB barrier. The application of non-corrosive silicone rubber, to the remaining edges, allowed a reservoir to be formed. 0.86 mol.dm^{-3} NaCl was introduced into the reservoir to initiate cathodic coating delamination.

Scanning Kelvin probe

Potentiometric measurements were obtained under atmospheric conditions using SKP instrumentation described in detail elsewhere [53]. The gold wire (125 μm diameter) SKP reference probe was vibrated normal to the sample surface at a vibration frequency of 280 Hz and amplitude of 40 μm. Ag/Ag^+, Cu/Cu^{2+}, Fe/Fe^{2+} and Zn/Zn^{2+} couples were used to perform calibration of the SKP following a procedure established previously [51, 53]. In short, metal discs (15 mm diameter, 5 mm thick) were machined to create 8 mm diameter, 1 mm deep wells. A 0.5 mol.dm^{-3} aqueous solution of each of the respective metal chloride salt (0.5 mol.dm^{-3} nitrate salt in the case of Ag) was then used to fill each well. The metal electrode potential (E_{corr}) was measured *vs.* SCE using a Solartron 1280 potentiostat, and then compared to the Volta potential difference measured between the SKP reference probe and the solution/air interface ($\Delta\Psi_{Sol}^{Ref}$). To account for the influence of PVB, 30 μm thick self-supporting polymer films were placed over each calibration well, in contact with the electrolyte meniscus. The Volta potential difference between the SKP reference probe and the polymer/air interface ($\Delta\Psi_{Pol}^{Ref}$) was obtained and Equation 5 was used to calculate the calibration constant (*C*).

$$E_{corr} = \Delta\Psi_{Pol}^{Ref} + C \qquad (V \; vs. SHE) \tag{5}$$

During cathodic delamination studies the SKP reference probe was scanned along a 12 mm line leading up to the defect/intact coating boundary. **Scans took place at regular intervals and repeated 4 times for each sample.** In both cases, Scans were recorded as numeric grids on the SKP control computer. **A constant humidity (~96% RH)** was achieved by use of open reservoirs of 0.86 mol.dm^{-3} NaCl, placed at the bottom of the chamber. An experimental temperature of 25 °C was maintained throughout.

3. Results

3.1 UV VIS Results

UV-VIS spectroscopy was used to characterise the pH dependent nature of BTA release from the ZnPhos-BTA pigment when dispersed in distilled water and 0.86 mol.dm^{-3} NaCl (aq) at varying pH. The UV absorption of BTA has been shown to be strongly dependent upon pH and under basic conditions a single peak ($\lambda_{max} = 274$ nm) is observed [55]. In the current work, the solution concentration of BTA (at any pH) was calculated by measuring the optical absorbance at 274 nm using Equation 3 and the values obtained are given in Table 1 and shown in Figure 1. The maximum (100 %) value assumes the complete release of BTA from the ZnPhos-BTA pigment, which, based on the 10 wt. % solution used, is estimated to be 8.4 x 10^{-4} mol.dm^{-3} Figure 1 shows that the release of BTA, from ZnPhos-BTA, is pH dependent. 44% of the BTA species is liberated when the ZnPhos-BTA pigment was dispersed in near neutral pH 7 solutions. The release efficiency falls to a minimum (9.2 %) at pH 11 and reaches a maximum at pH 13 (96%). In the presence of NaCl, the release efficiencies were reduced at every pH value.

(Table 1)
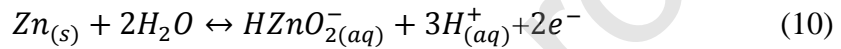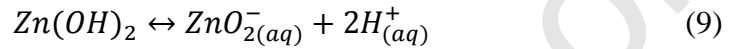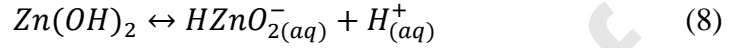
(Figure 1)

3.2 Cathodic Delamination Results

Having characterized the pH dependent release of BTA from the ZnPhos-BTA pigment, a systematic study was undertaken with the aim of determining the effect of the pigment on the kinetics and mechanism of cathodic delamination.

The corrosion driven cathodic delamination of unpigmented PVB, from a HDG substrate, was initially studied to obtain baseline kinetics. The mechanism by which unpigmented PVB cathodically delaminates from a HDG substrate has been published on numerous occasions previously [53, 56]. Time dependent $E_{corr}(x)$ profiles became established shortly after initiation (t_i) and are shown in Figure 2. A uniform potential value of -0.30 V vs. SHE **is observed in Region IV,** determined by the relative rates of anodic zinc dissolution (Equation 6) and the **oxygen reduction reaction** (ORR) (Equation 7), is associated with the intact coating (E_{intact}) [53, 56]. Here the ORR is kinetically fast, whilst the anodic reaction is slowed by the zinc hydr(oxide) layer. The presence of the corrosive NaCl electrolyte in the defect region results in dissolution of this hydr(oxide) film. The E_{corr} value falls to be in line with that expected for freely corroding zinc (ca. -0.7 V vs. SHE) [53, 56].

$$Zn_{(s)} \leftrightarrow Zn^{2+}_{(aq)} + 2e^- \tag{6}$$

$$O_2 + 2H_2O + 4e^- \leftrightarrow 4OH^-_{(aq)} \tag{7}$$
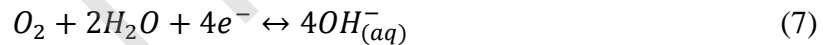
A sharp deflection in the profile (Region III) is observed between high (intact) and low (defect) potential values. This transition is a convenient way by which to determine the distance between the artificial coating defect, and the point to which the coating has become delaminated (delamination front, x_{del}) and can subsequently be used to determine the coating disbondment kinetics. The ingress of alkali (pH ≥10) electrolyte into the underfilm region [56] results in the dissolution of zinc hydr(oxide) to soluble hydrogen zincate (Equation 8) or zincate (Equation 9) [53, 56] and at pH > 10.37 zinc dissolves via Equation 10. The formation of zincate causes a decrease in potential. However, the region can still be considered as a net cathode and the potential values observed are greater than

those in Region I. The occurrence of cathodic oxygen reduction reaction (ORR) results in dissolution of the zinc hydr(oxide), as well as base catalyzed hydrolysis of vinyl acetate functions within the PVB, both of which contribute to the ultimate disbondment and failure of the coating [56]. A linear gradient in potential is observed in Region II and this is associated with ohmic ion current flux in the underfilm electrolyte.

$$Zn(OH)_2 \leftrightarrow HZnO_{2(aq)}^- + H_{(aq)}^+ \tag{8}$$

$$Zn(OH)_2 \leftrightarrow ZnO_{2(aq)}^- + 2H_{(aq)}^+ \tag{9}$$

$$Zn_{(s)} + 2H_2O \leftrightarrow HZnO_{2(aq)}^- + 3H_{(aq)}^+ + 2e^- \tag{10}$$

(Figure 2)

ZnPhos based pigments; The effect of ZnPhos on the rate of PVB coating disbondment was investigated by systematically changing the ZnPhos ϕ (present within the coating) from 0.05 to 0.2. The time dependent $E_{corr}(x)$ profiles obtained for each ZnPhos ϕ are shown in Figure 3.

Table 2 shows t_i and E_{intact}, obtained from Figure 3, for each of the values of ZnPhos ϕ. There is some evidence that ZnPhos results in a delay in the onset of cathodic disbondment, and t_i increases to 420 minutes for 0.1 ϕ ZnPhos. However, it should be borne in mind that the SKP is unable to take measurements immediately up to the defect, and the time after which the establishment of E_{corr} profiles is first detected (initiation time) is therefore associated with some error. There is some indication that ZnPhos acts to suppress the value of E_{corr} in the absence of cathodic delamination (the value measured over the intact coating, E_{intact}). The meaning of E_{intact} has been explained on previous occasions. In brief, for non-conducting polymers, the intact potential (E_{intact}) represents the open circuit potential of the

(oxide covered) metal (zinc) surface. This value can be influenced by both atmospheric O_2 and Bronsted acid-base reactions which take place between the surface oxide and the coating [57-60]. E_{intact} is ~ -0.39 V vs. SHE for coatings containing 0.2 ϕ ZnPhos, compared to ~-0.27 V vs. SHE for unpigmented coatings. On the basis of mixed potential theory the decrease in potential (Figure 3) suggests that ZnPhos behaves as a net cathodic inhibitor. There is some evidence of a time dependent increase in potential within the near defect region at 0.05 ZnPhos ϕ. However, this trend is not observed for higher values of ϕ.

(Figure 3)

(Table 2)

Coating disbondment kinetics can be obtained from Figure 4, which shows x_{del} as a function of the associated delamination time ($t_{del} - t_i$) for all ZnPhos ϕ. The diffusion length is quite small in the initial time period of the experiment and cation diffusion in the underfilm electrolyte cannot be rate limiting [51]. The initial, linear rates were therefore estimated by construction of a tangent to the x_{del} vs. $(t_{del} - t_i)$ curves at $(t_{del} - t_i) = zero$, and allowed for convenient comparison with ZnPhos-BTA. The linear delamination rate constant k_{del} values obtained are shown in Table 2.The curves in Figure 4 appear to show that x_{del} increases with $t^{1/2}$ This is expected in the case that kinetics are parabolic (as is typical for uninhibited organic coating systems in the absence of pigments etc.) and that the rate of coating delamination are controlled by the ionic conductivity and mobility of cations (here Na^+) in the under-film electrolyte [52]. Although the cathodic delamination rates shown in Figure 4 decrease with increasing ZnPhos, the kinetics of cathodic delamination appear to remain parabolic.

(Figure 4)

ZnPhos-BTA based pigments; Figure 5 shows E_{corr} as a function of x_{del} for a PVB coating

containing 0.01-0.1 ϕ ZnPhos-BTA. As with ZnPhos, an increase in ZnPhos-BTA ϕ tends

to result in a general increase in the time before onset of delamination (Table 3), which

occurs almost immediately in the absence of ZnPhos-BTA and occurs after 2100 minutes

at 0.1 ϕ ZnPhos-BTA. The presence of ZnPhos-BTA also appears to result in a further

suppression (compared to ZnPhos) in E_{intact} to ~ -0.5 V vs. SHE (Figure 6). **The reduction**

in E_{intact} observed at 0.1 ϕ is similar to that observed for the cationic BTA pigment

studied previously [49], for which the change in E_{intact} is around -150 mV. On the basis

of mixed potential theory, the slight depression of time-independent E_{intact} values, with

increasing PVF, is consistent with the pigment acting to inhibit cathodic processes

and/or facilitate anodic processes occurring at the coating-zinc interface. Again, the

potential recorded within the near defect region generally appears to increase with time for

some values of ZnPhos-BTA ϕ.

(Figure 5)

(Figure 6)

Figure 7 shows x_{del} plotted as a function of t_{del}-t_i for varying values of ZnPhos-BTA ϕ. The

initial k_{del} values obtained from Figure 5 are also shown in Table 3 and **decreases** from 1.5

μm.min^{-1} for coatings containing 0.01 ϕ ZnPhos-BTA, to 0.5 μm.min^{-1} for coatings

containing 0.1 ϕ ZnPhos-BTA . Linear kinetics are observed for all values of ZnPhos-BTA

ϕ. In contradistinction to ZnPhos, Zn-BTA appears to both reduce the rate of cathodic

delamination, and change the mechanism of delamination in such a way that its rate

becomes controlled by interfacial electron transfer. A change in delamination mechanism

has been observed previously during a study into the use of divalent cation exchanged

bentonites [61] and cross-linked sulphonated polystyrene [62] to inhibit corrosion driven coating disbondment from HDG. Whilst the use of Ca^{2+} and Zn^{2+} ions both resulted in a decrease in delamination rate, only Zn^{2+} caused a change in delamination kinetics from parabolic to linear.
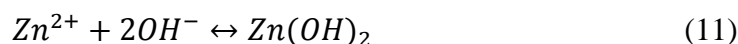
(Figure 7)

(Table 3)

Figure 8 shows the linear delamination rate constant k_{del} obtained for varying concentrations of ZnPhos and ZnPhos-BTA. **Previously obtained values for strontium chromate (which exhibits a similar density to ZnPhos, 3.9 g.cm^{-3}) are also shown for comparison [53].** The efficiency of ZnPhos-BTA is equivalent to that achieved by strontium chromate, particularly at ϕ values of less than 0.1.
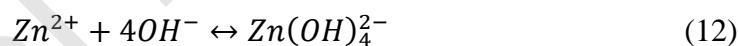
(Figure 8)

4. Discussion

ZnPhos was only able to inhibit cathodic disbondment of a PVB coatings from HDG to a limited extent, and whilst its ability to behave as a corrosion inhibitor has been investigated extensively elsewhere [9-14, 21-22, 24-27], its low solubility ($Zn_3(PO_4)_2$ $K_{sp} = 9$ x 10^{-33} mol^{5}dm^{-15}) [23] tends to limit its performance. Previous work has shown that Zn^{2+} ions, present in the underfilm electrolyte, are capable of buffering the pH, this in turn preventing zinc(hydr)oxide dissolution via Equation 8 and Equation 9 [62]. Another possibility is that the Zn^{2+} ions reinforce the hydr(oxide) layer via Equation 11 (K_{sp} =3.1x10^{-14} mol^3 dm^{-9}) [23]. However, both of these possibilities would give rise to a reduction in interfacial

electron transfer and linear delamination kinetics, and it therefore seems plausible that insufficient Zn^{2+} is released from the poorly soluble ZnPhos.

$$Zn^{2+} + 2OH^- \leftrightarrow Zn(OH)_2 \qquad (11)$$

In this work, although the rate of PVB cathodic delamination decreases with increasing ZnPhos ϕ (Figure 4), the kinetics of cathodic delamination appear to remain parabolic. There are two plausible reasons for this; 1.) there is an increase in the resistance of the underfilm electrolyte and/or 2.) there is a change in the constant of proportionality between the cell current and the rate of disbondment/unit area, which may occur, for example, due to chemical changes at the metal/coating interface. The second possibility may come about if the pH in the underfilm electrolyte were buffered, for example via Equation 12 and 13. This, in turn, would lead to a reduction in the rate of dissolution of the zinc hydr(oxide), as well as base catalyzed hydrolysis of vinyl acetate functions within the PVB, both of which contribute to the ultimate disbondment and failure of the coating [56].

$$Zn^{2+} + 4OH^- \leftrightarrow Zn(OH)_4^{2-} \qquad (12)$$

$$Zn_3(PO_4)_2 + 12OH^- \leftrightarrow 3Zn(OH)_4^{2-} + 2PO_4^{3-} \qquad (13)$$
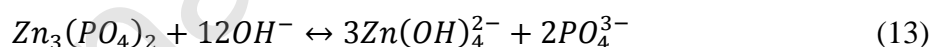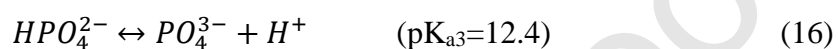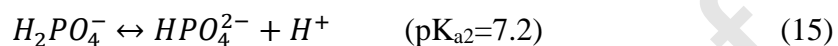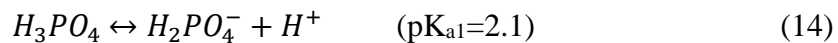
Whilst it is not possible to categorically determine the exact reason for the reduction in the parabolic rate of delamination, what is clear is that the rate of cathodic delamination does not become determined by interfacial electron transfer.

The efficiency of ZnPhos [8-14, 21-22, 24-27] and BTA [28-34, 37-40,42-50] corrosion inhibitors, when used in isolation, has been investigated extensively elsewhere and the ability of ZnPhos-BTA based pigments to inhibit the corrosion of iron has been demonstrated previously [50]. During that work it was proposed that heat, produced during

the production of ZnPhos from zinc nitrate and sodium phosphate, was used to dissolve and recrystalise BTA during the co-precipitation. The ZnPhos-BTA pigment formed was shown to have a plank martensite structure and this was believed to reinforce the combination of the pigments to epoxy coatings [50]. The stability of the coating was attributed to formation of N-Zn bonds [50]. However, to the authors' knowledge, the work described herein provides the first account of the ability of a ZnPhos-BTA inhibitive pigment (produced by adsorbing BTA onto ZnPhos) to act as an effective inhibitor of the corrosion of HDG. The way in which BTA acts in combination with ZnPhos to inhibit organic coating delamination on HDG is, as yet, uncertain. Although there is some evidence that the presence of ZnPhos-BTA results in a time dependent increase in the potential value recorded within the near defect region (Figure 3). The limited solubility of zinc phosphate limits significant release of the constituent ions into the defect electrolyte at the coating defect interface. It is therefore deemed unlikely that the inhibition of anodic zinc dissolution (within the defect site) plays a significant role in the inhibition mechanism. For all ϕ values the zinc in the defect region became heavily corroded, and due to the large size of the defect region (~1 cm^2) only a very **limited concentration** of ZnPhos-BTA will be available at the anodic site and it is unlikely that anodic current distributions will become rate determining.

The formation of a Zn-BTA complex (in preference to ZnPhos) has been shown to occur in the case that Zn is exposed to a BTA containing phosphate electrolyte [30]. In the same work, the addition of 10 mmol.dm^{-3} BTA was shown to result in the removal of the phosphate layer on the surface of Zn which had been pre-exposed to phosphate [30] and it therefore seems reasonable to propose the formation of a similar complex in our work. There appears to be two plausible explanations to explain the formation of Zn-BTA; 1.) via

salt formation or 2.) via surface chemisorption. The first possibility pertains to a mechanism by which BTA can adsorb onto, and indeed release from, a ZnPhos surface as a result of an acid base reaction. The pH dependent speciation of H_3PO_4 proceeds according to the following dissociation reactions (Equation 14-16) [63].

$$H_3PO_4 \leftrightarrow H_2PO_4^- + H^+ \qquad (pK_{a1}=2.1) \qquad (14)$$

$$H_2PO_4^- \leftrightarrow HPO_4^{2-} + H^+ \qquad (pK_{a2}=7.2) \qquad (15)$$

$$HPO_4^{2-} \leftrightarrow PO_4^{3-} + H^+ \qquad (pK_{a3}=12.4) \qquad (16)$$

Assuming phosphoric acid exists as its conjugate base (PO_4^{3-}), and by considering the pKa values associated with the protonic equilibria linking the BTA species (Equation 1 and 2), it seems reasonable to suggest that an acid-base proton exchange reaction occurs according to Equation 17.

$$PO_4^{3-} + HBTA \leftrightarrow HPO_4^{2-} + BTA^- \qquad (17)$$
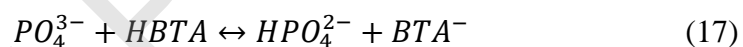
Following this logic, it is believed that BTA reacts with ZnPhos via Equation 18. It is plausible that the higher solubility of the modified ZnPhos structure increases its corrosion inhibiting efficiency [8, 50].

$$Zn_3(PO_4)_2 + 2HBTA \leftrightarrow Zn(BTA)_2 + 2ZnHPO_4 \qquad (18)$$

The second possibility, surface chemisorption, is shown by the simplified schematic in Figure 9 and involves a mechanism whereby protonation of surface phosphate tri-anion results in the formation of hydrogen phosphate anions which remain associated to the surface. Electrostatic attraction then occurs between the positively charged metal salt surface and the resultant BTA$^-$.

(Figure 9)

In the presence of chloride ions it is then feasible to propose that the ZnPhos-BTA behaves **as an** ion-exchange medium **according to** Equation 19.

$$Zn(BTA)_2 + 2Cl^- \rightarrow ZnCl_2 + 2BTA^- \tag{19}$$
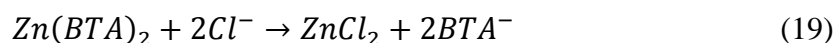
However, if the preceding scenario were true, increased BTA release efficiencies from the ZnPhos-BTA pigment would be expected in the presence of free chloride ions. The measurements reported in Table 1 reveal that the presence of NaCl seemingly inhibits the liberation of BTA species from the ZnPhos-BTA pigment. The reduction in the release efficiencies in the presence of NaCl may be attributed to the 'salting out' phenomenon [64]. In this scenario, solvent water molecules are electrostatically attracted to the dissolved salt ions in solution, thereby reducing the availability and capacity for the water molecules to interact with the adsorbed BTA species. Consequently, anion exchange is not believed to occur to any significant degree **for this system**.

The pH dependent release of BTA species is plotted in Figure 1. The release of the BTA species from ZnPhos-BTA (via Equation 18) reaches a minimum between pH 10 and 11. The pH dependent K_{sp} values, for the Zn(BTA)$_2$ complex, calculated using Equation 20, along with the measured BTA concentrations found in Table 1, are tabulated in Table 4.

$$K_{sp} = [Zn^{2+}][BTA^-]^2 \tag{20}$$

Please note that the K_{sp} values given are calculated with the assumption that all of the Zn^{2+}cations form during the dissolution of the Zn(BTA)$_2$ complex. However, it should be considered that the actual values of [Zn^{2+}] may, in fact, be higher due to the

dissolution of ZnPhos, which will result in the release of Zn^{2+} cations and phosphate anions into solution.

Table 4 shows that, of the pH values included, the $Zn(BTA)_2$ complex exhibits the lowest calculated K_{sp} value of 2.2×10^{-13} $mol.dm^{-3}$ at pH 11. It is likely that the minima observed at pH values 10 and 11 is associated with the limited solubility of Zn^{2+} (K_{sp} is 3.1×10^{-13} $mol.dm^{-9}$ [23]) at these conditions. At pH 11 any Zn^{2+} released from $Zn(BTA)_2$ complex would immediately precipitate out as solid $Zn(OH)_2$ [65], as the $[Zn^{2+}]$ threshold is exceeded (3.1×10 10^{-8} $mol.dm^{-3}$).

At pH 7 (below pK_{a2} value of BTA (8.2)) benzotriazole predominantly exists as BTAH (Equation 2). The notably higher release efficiency of BTA at pH 7 is therefore likely to be a result of the relatively high solubility of BTAH, 20 $g.dm^{-3}$ [66]. The near total release of BTA observed at pH 13 reflects that both H_3PO_4 (Equations 14-16) and BTAH (Equations 1-2) species are fully dissociated and. **The pH dependent solubility equilibrium of the BTA species is shown schematically in Figure 10.**

(Table 4)

(Figure 10)

Despite the variation in release efficiencies, the results in section 3.2 demonstrate that the ZnPhos-BTA pigment can effectively inhibit cathodic disbondment on HDG. It is expected that the environment of the coating defect interface/cathodically disbonding front will have an associated pH of between 10-11 [56]. Thus, the limited release of BTA from the ZnPhos-BTA pigment at the relevant pH values is sufficient to effectively inhibit cathodic

disbondment. It may also be the case that, at the onset of cathodic disbondment and prior to the establishment of the elevated pH region, a proportion of BTA is liberated from the pigment in the near neutral electrolyte, as demonstrated in the release measurements at pH 7 (Figure 1), and contribute to the inhibition.

Despite the efficiency with which BTA itself is known to inhibit corrosion, the exact mechanism by which it is able to do so is, as yet, uncertain [37-38, 67]. This ambiguity is a result of the various pH dependent phenomena which can occur at the surface of a metal undergoing corrosion. In the case of transition metals such as Fe and Zn there are two mechanistic theories which predominate, the first of which involves the adsorption of the BTAH species onto the substrate during the reaction given by Equation 21 where $M_{(s)}$ is an atom at the surface of the metal [67-70]. In this manner, the adsorbed BTAH layer physically disrupts the adsorption of aggressive ions, such as Cl$^-$, thereby hindering the onset of corrosion failure mechanisms such as the dissolution of an oxide film.

$$[BTAH]_{aq} + M_s \rightarrow [BTAH]_{ads}:M \tag{21}$$
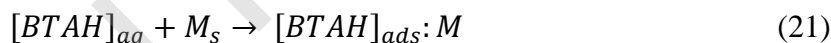
A densely packed polymeric film is believed to form during the second mechanism which involves the precipitation of a metal-BTA complex via Equation 22 [67-72]. This complex would inhibit corrosion in a similar manner to the above mechanism but would also likely hinder electron transfer reactions at the surface, on account of the more robust densely packed film [49].

$$M_{(s)} + BTAH \rightarrow MBTA + H^+ + e^- \qquad pK_a \sim 8.2 \ BTAH \tag{22}$$

$$n(MBTA) \rightarrow (MBTA)_n \tag{23}$$
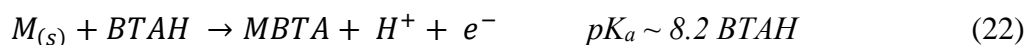
Adsorption (Equation 21) and complex formation (Equation 22) are believed to occur in equilibrium (Equation 24) [73-74]. This implies that Equation 22 is favoured at higher pH values consistent with those measured in the underfilm electrolyte of a zinc cathodic disbondment cell (pH~11) [56] and it therefore seems reasonable to propose that organic coating disbondment is predominantly inhibited by the formation of a BTA-derived polymeric complex in this work.

$$nBTAH_{ads} + nM \leftrightarrow (MBTA)_n + nH^+ + ne^- \tag{24}$$
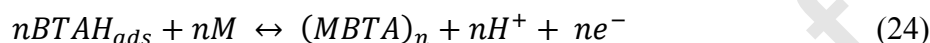
Thus, in the case of Zn^{2+} ions, an expected BTA-derived polymeric complex is given in Equation (25).

$$2BTAH + Zn^{2+} \leftrightarrow Zn(BTA)_2 + 2H^+ \tag{25}$$
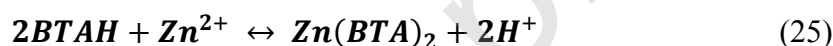
It is, of course, entirely plausible that the availability of Zn^{2+} ions plays a role in the enhanced delamination resistance observed in the case of coatings which contain ZnPhos-BTA. Zn^{2+} ions have been shown to retard the delamination rate of PVB from HDG by a factor of six [62].However, the reduced inhibitor efficiency exhibited by ZnPhos, alongside the known ability of BTA to behave as an anodic corrosion inhibitor, means that we can be confident that the higher efficiency observed for ZnPhos-BTA is a consequence of the **presence** of BTA.

5. Conclusions

This paper demonstrates a methodology by which to produce a novel, zinc phosphate-benzotriazole corrosion inhibitor pigment during a process whereby benzotriazole (BTA) is adsorbed onto zinc phosphate (ZnPhos) using a simple, easily scalable rotary evaporation process. UV-VIS spectroscopy was used to measure the release efficiency of BTA from the ZnPhos-BTA pigment in a range of pH modified and NaCl containing solutions. The

results showed that, the BTA release is moderately efficient at pH 7 (44%), the least efficient at pH 11 (~9%), and most efficient at pH 13 (96%).

The scanning Kelvin probe (SKP) was used to monitor the corrosion driven cathodic coating delamination of both a ZnPhos and ZnPhos-BTA containing PVB coating from a hot dip galvanized steel (HDG) substrate. It was found that;

- The rate of corrosion driven coating disbondment of a PVB coating from HDG decreased as the pigment volume fraction of ZnPhos (present within the coating) was systematically varied between 0.05 and 0.2. The kinetics of cathodic delamination remained parabolic for all concentrations investigated. The reduction in rate is therefore believed to be a result of 1.) an increase in the resistance of the underfilm electrolyte and/or 2.) a change in the constant of proportionality between the cell current and the rate of disbondment/ unit area.

- In the presence of ZnPhos-BTA the rate of delamination is reduced compared to that obtained when ZnPhos is used in isolation. The rate of delamination becomes controlled by interfacial electron transfer.

- For both ZnPhos and ZnPhos-BTA, a suppression in E_{intact}, consistent with net cathodic inhibition, is observed.

- Two mechanisms are proposed to explain the process by which BTA is able to adsorb onto ZnPhos; the first based on the formation of a Zn-BTA salt, and the second on chemisorption of BTA onto the ZnPhos surface.

This paper demonstrates the potential for pre-existing industry standard corrosion inhibitor technologies, such as inorganic ZnPhos systems, to be utilized in conjunction with known

organic corrosion inhibitors such as BTA to provide significantly enhanced performance

when incorporated within protective organic coatings.

Authors contribution

N. Wint: Validation, formal analysis, investigation, data curation, writing-original & draft, writing- review and editing, visualization, supervision.
C. M. Griffiths: Validation, formal analysis, investigation, data curation.
C.A.J. Richards: Validation, formal analysis, investigation, data curation, writing-original & draft, writing- review and editing, visualization.
G.Williams: Conceptualization, methodology, writing- review and editing, supervision
H.N. McMurray: Conceptualization, methodology, writing- review and editing, supervision

Declaration of interests
The authors declare that they have no known competing financial interests or personal relationships that could have appeared to influence the work reported in this paper.

5. Acknowledgments

The raw/processed data required to reproduce these findings cannot be shared at this time as the data also forms part of an ongoing study.

6. References

[1] J. Sander, Coil Coating, Vincentz, Hanover (2014).

[2] G.Williams, H. N.McMurray, Underfilm/coating corrosion, in: B. R. A. Cottis,M.

Graham, R. Lindsay, S. Lyon, T. J. A. Richardson, D. J. D. Scantlebury, H. Stott, (Eds.),

Shreir's Corrosion, Elsevier Science, 2009, pp. .988-2004.

[3] U.S. Environmental Protection Agency, Health Assessment Document for Chromium, Final Report, EPA-600/8-83-01 4F (2019).

[4] S. A. Katz, H. Salem, The toxicology of chromium with respect to its chemical speciation: a review. Journal of Applied Toxicology. 13 (1993) 217-224. https://doi.org/10.1002/jat.2550130314.

[5] S. Langard, T. Norseth, Occurrence of lung cancer in workers producing chromium pigments, British Journal of Industrial Medicine. 40 (1983) 71-74 https://doi.org/ 10.1136/oem.40.1.71.

[6] A. Sheffet, I. Thind, A. M. Miller, D. B. Louria, Cancer mortality in a pigment plant utilizing lead and zinc chromates, Archives of Environmental Health: An International Journal. 37 (1982) 44-52. https://doi.org /10.1080/00039896.1982.10667532.

[7] B. Ramezanzadeh, E. Ghasemi, F. Askari, M. Mahdavian, Synthesis and characterization of a new generation of inhibitive pigment based on zinc acetate/benzotriazole: Solution phase and coating phase studies, Dyes and Pigments, 122 (2015) 331-345. https://doi.org/10.1016/j.dyepig.2015.07.013.

[8] F. Askari, E. Ghasemi, B. Ramezanzadeh, M. Mahdavian, Potassium Zinc Phosphate Pigment Coupled with Benzotriazole for Enhanced Protection of Carbon Steel, Corrosion. 72 (2016) 1526-1538. https://doi.org/10.5006/2086.

[9] S. Dalbin, G. Maurin, R. P. Nogueira, J. Persello, N. Pommier, Surface and Coatings Technology.194 (2005) 363-371. https://doi.org/10.1016/j.surfcoat.2004.07.126.

[10] K. Aramaki, The inhibition effects of chromate-free anion inhibitors on corrosion of zinc in aerated 0.1 M NaCl, Corrosion Science. 43 (2001) 591-604. https://doi.org/10.1016/S0010-938X(00)00085-8.

[11] R. Berger, U. Bexell, T. M. Grehk, S. E. Hornstrom, A comparative study of the corrosion protective properties of chromium and chromium free passivation methods, Surface and Coatings Technology. 202 (2007) 391-397. https://doi.org/10.1016/j.surfcoat.2007.06.001.

[12] M. F. Montemor, Functional and Smart Coatings for Corrosion protection: A review of recent advances, Surface and Coatings Technology. 258 (2014) 17-37. https://doi.org/10.1016/j.surfcoat.2014.06.031.

[13] P. Puomi, H. M. Fagerholm, J. B. Rosenholm, K. Jyrkas, Comparison of different commercial pretreatment methods for hot-dip galvanized and Galfan coated steel, Surface and Coatings Technology. 115 (1999) 70-78. https://doi.org/10.1016/S0257-8972(99)00170-X.

[14] P. Puomi, H. M. Fagerholm, A. Sopanen, Parameters affecting long term performance of painted galvanised steel, Anti-Corrosion Methods and Materials. 48 (2001) 160-171. https://doi.org/10.1108/00035590110391076.

[15] M. Zubielewicz, W. Gnot, Mechanisms of non-toxic anticorrosive pigments in organic waterborne coatings, Progress in Organic Coatings. 49 (2004) 358–371, doi:10.1016/j.porgcoat.2003.11.001

[16] M. Bethencourt, F.J. Botana, M. Marcos, R.M. Osuna, J.M. Sánchez-Amaya, Inhibitor properties of "green" pigments for paints, Progress in Organic Coatings. 46 (2003) 280–287, doi:10.1016/S0300-9440(03)00013-4.

[17] J. Davis, Corrosion: Understanding the Basics, vol.20, Materials Park: ASM International, 2000, pp. 47-51.

[18] M. Pryor, M. Cohen, The inhibition of the corrosion of iron by some anodic inhibitors. Journal of the Electrochemical Society. 100 (1952) 203-215.

[19] J. Mayne, Paints for the Protection of Steel- a Reviw of Reseach into their Modes of Action. British Corrosion Journal. 5 (1970) 106-111.

[20] D. Weng, P. Jpkiel, A. Uebleis, H. Boehni, Corrosion and protection characteristics of zinc and manganese phosphate coatings, Surface and Coatings Technology. 88 (1996) 147-156.

[21] M. Mahdavian, M.M. Attar, Evaluation of zinc phosphate and zinc chromate effectiveness vas AC and DC methods, Progress in Organic Coatings. 53 (2005) 191-194. https://doi.org/10.1016/j.porgcoat.2005.02.007.

[22] M. Beiro, A. Collazo, M. Izquierdo, X. No´voa, C. Pérez, Characterisation of barrier properties of organic paints: the zinc phosphate effectiveness, Progress in Organic Coatings. 46 (2003) 97-106. https://doi.org/10.1016/S0300-9440(02)00216-3.

[23] D. R. Lide, CRC Handbook of Chemistry and Physics, 84th Edition, CRC Press (2003).

[24] J. Sinko, Challenges of chromate inhibitor pigments replacement in organic coatings, Progress in Organic Coatings. 42 (2001) 267-282. http://doi.org/ 10.1016/S0300-9440(01)00202-8.

[25] J.A. Burkill, J.E.O. Mayne, The limitations of zinc phosphate as an inhibitive pigment, JOCCA. 9 (1988) 273–285.

[26] A. Amirudin, C. Barreau, R. Hellouin, D. Thierry, Evaluation of anti-corrosive pigments by pigment extract studies, atmospheric exposure and electrochemical impedance spectroscopy, Progress in Organic Coatings. 25 (1995) 339-355. https://doi.org/10.1016/0300-9440(94)00546-D.

[27] M. S. Ghaffari, R. Naderi, M. Sayehbani, The effect of mixture of mercaptobenzimidazole and zinc phosphate on the corrosion protection of epoxy/polyamide coating, Progess in Organic Coatings. 86 (2015) 117-124. https://doi.org/10.1016/j.porgcoat.2015.04.020.

[28] Y. Kuznetsov, L. P. Podgornova, L.P., Zinc Protection in Alkaline Phosphate Solutions by Benzimidazoles, Zashch. Met.21 (1985) 487.

[29] Y. Kuznetsov, L. P. Podgornova, L. P. Kazanskii, Chemical structures of benzoimidazoles and their protective effects on zinc and copper in phosphate electrolytes, Zashch. Met. 40 (2004) 142.

[30] L. P. Kazanskii, E. M. Sokolova, Y. E. Pronin, Adsorption of 1, 2, 3-Benzotriazole on Zinc surface from Phosphate Solution, Protection of Metals and Physical Chemistry of Surfaces. 49 (2013) 844-853. https://doi.org/10.1134/S2070205113070101.

[31] T. Hashemi, C. A. Hogarth, The mechanism of the corrosion inhibition of copper in NaCl by benzotriazole studied by electron spectroscopy, Electrochimica Acta. 33 (1988)1123-1127. https://doi.org/10.1016/0013-4686(88)80203-2

[32] V. Sirtori, F. Zambon, L. Lombardio, XPS and Ellipsometric Characterization of Zinc-BTA Complex, Journal of Electronic Materials. 29 (2000) 463-467. https://doi.org/10.1007/s11664-000-0162-9.

[33] K. Aramaki, Effects of organic inhibitors on corrosion of zinc in an aerated 0.5 M NaCl solution, Corrosion Science. 43 (2001) 1985-2000. https://doi.org/10.1016/S0010-938X(00)00174-8.

[34] M. Fenelon, C. B. Breslin, An Electrochemical study of the formation of Benzotriazole surface films on Copper, Zinc and a Copper–Zinc alloy, Journal of Applied Electrochemistry. 31 (2001) 509-516. https://doi.org/10.1023/A:1017503031045.

[35] T. Kosec, I. Milošev, B. Pihlar, Benzotriazole as an inhibitor of brass corrosion in chloride solution, Applied Surface Science. 253 (2007) 8863-8873. https://doi.org/10.1016/j.apsusc.2007.04.083.

[36] T. Kosec, T. D. Kek, Merl, I. Milošev, Impedance and XPS study of benzotriazole films formed on copper, copper–zinc alloys and zinc in chloride solution, Corrosion Science. 50 (2008) 1987-1997. https://doi.org/10.1016/j.corsci.2008.04.016.

[37] M. Finšgar, I. Milošev. Inhibition of copper corrosion by 1,2,3-benzotriazole: A review, Corrosion Science, 52 (2010) 2737–2749. https://doi.org/10.1016/j.corsci.2010.05.002.

[38] N. Kovačević, A. Kokalj, Chemistry of the interaction between azole type corrosion inhibitor molecules and metal surfaces, Materials Chemistry and Physics. 137 (2012) 331–339. https://doi.org/10.1016/j.matchemphys.2012.09.030.

[39] T. J. Harvey, F. C. Walsh, A.H. Nahlé, A review of inhibitors for the corrosion of transition metals in aqueous acids, Journal of Molecular Liquids. 266 (2018) 160–175. https://doi.org/10.1016/j.molliq.2018.06.014.

[40] K. Xhanari, M. Finšgar. Organic corrosion inhibitors for aluminum and its alloys in chloride and alkaline solutions: A review, Arabian Journal of Chemistry, (2016). https://doi.org/10.1016/j.arabjc.2016.08.009.

[41] A. Seeland, M. Oetken, A. Kiss, E. Fries, J. Oehlmann, Acute and chronic toxicity of benzotriazoles to aquatic organisms, Environ Sci Pollut Res. 19 (2012)1781–1790. doi:10.1007/s11356-011-0705-z.

[42] D. A. Pillar, J. S. Cornell, D. L. Dufresne, M. T. Hernandez, Toxicity of benzotriazole and benzotriazole derivatives to three aquatic species, Wat. Res. 35 (2001) 557-560, doi:10.1016/S0043-1354(00)00268-2.

[43] G. Williams, H. N. Mcmurray, Inhibition of filiform corrosion on organic-coated AA2024-T3 by smart-release cation and anion-exchange pigments, Electrochemica Acta. 69 (2012) 287–294. https://doi.org/1-.1016/j.electacta.2012.03.002.

[44] G. Markevicius, S. Chaudhuri, C. Bajracharya, R. Rastogi, J. Xiao, C. Burnett, T.Q. Chastek, Polyoligomeric silsesquioxane (POSS)–hydrogenated polybutadiene polyurethane coatings for corrosion inhibition of AA2024, Progress in Organic Coatings. 75 (2012) 319-327. https://doi.org/10.1016/j.porgcoat.2012.08.001.

[45] M. Serdechnova, A. N. Salak, F. S. Barbosa, D. E.L. Vieira, J. Tedim, M. L. Zheludkevich, M. G. S. Ferreira, Interlayer intercalation and arrangement of 2-mercaptobenzothiazolate and 1,2,3-benzotriazolate anions in layered double hydroxides: In situ X-ray diffraction study, Journal of Solid State Chemistry. 233 (2016) 158-165. https://doi.org/10.1016/j.jssc.2015.10.023.

[46] G. Williams, H. N. McMurray. Inhibition of Filiform Corrosion on Polymer Coated AA2024-T3 by Hydrotalcite-Like Pigments Incorporating Organic Anions. Electrochemical and Solid-State Letters. 7 (2004) B13-B15.

[47] N. Cotolan, S. Varvara, E. Albert, G. Szabó, Z. Hórvölgyi, L.-M. Mureşan, Evaluation of corrosion inhibition performance of silica sol–gel layers deposited on galvanised steel, Corrosion Engineering, Science and Technology. 51 (2016) 373-382. https://doi.org/10.1080/1478422X.2015.1120404.

[48] K. Kamburova, N. Boshkova, N. Boshkov, Ts. Radeva, Design of polymeric core-shell nanocontainers impregnated with benzotriazole for active corrosion protection of galvanized steel, Colloids and Surfaces A: Physicochemical and Engineering Aspects. 499 (2016) 24-30. https://doi.org/10.1016/j.colsurfa.2016.03.067.

[49] C. A. J. Richards, H. N. McMurray, G. Williams, Smart-release inhibition of corrosion driven organic coating failure on zinc by cationic benzotriazole based pigments, Corrosion Science. 154, 101-110 (2019). https://doi.org/10.1016/j.corsci.2019.04.005.

[50] M. Miao, X.-Y. Yuan, X.-G. Wang, Y. Lu, J.-K. Liu, One step self-heating synthesis and their excellent anticorrosion performance of zinc phosphate/benzotriazole composite

pigments, Dyes and Pigments. 141 (2017) 75-82.

https://dx.doi.org/10.1016/j.dyepig.2017.01.060.

[51] A. Leng, H. Streckel, M. Stratmann, The delamination of polymeric coatings from steel. Part 1: Calibration of the Kelvinprobe and basic delamination mechanism, Corrosion Science. 41 (1999) 547-578. https://doi.org/10.1016/S0010-938X(98)00166-8.

[52] A. Leng, H. Streckel, and M. Stratmann, The delamination of polymeric coatings from steel. Part 2: First stage of delamination, effect of type and concentration of cations on delamination, chemical analysis of the interface, Corrosion Science. 41 (1999) 579-597. https://doi.org/10.1016/S0010-938X(98)00167-X

[53] G. Williams, H.N. McMurray, Chromate Inhibition of Corrosion-Driven Organic Coating Delamination Studied Using a Scanning Kelvin Probe Technique, Journal of the Electrochemical Society. 148 (2001) B377-B385. https://doi.org/ doi:10.1149/1.1396336.

[54] G. Wypych, PHOTOPHYSICS, 1-25. (2013), 10.1016/B978-1-895198-62-1.50004-4

[55] J. E. Fagel, G. W. Ewing, The Ultraviolet Absorption of Benzotriazole, Journal of the American Chemical Society. 73 (1951) 4360-4362.

[56] W. Fürbeth, M. Stratmann, The delamination of polymeric coatings from electrogalvanised steel – a mechanistic approach.: Part 1: delamination from a defect with intact zinc layer, Corrosion Science. 43 (2001) 207-227. https://doi.org/10.1016/S0010-938X(00)00047-0.

[57] G. Williams, A. Gabriel, A. Cook, H. N. McMurray, Dopant Effects in Polyaniline Inhibition of Corrosion-Driven Organic Coating Cathodic Delamination on Iron, Journal

of the Electrochemical Society. 153 (2006) B425-B433.

https://doi.org/10.1149/1.2229280.

[58] R. J. Holness, G. Williams, D. A. Worsley, H. N. McMurray, Polyaniline Inhibition of Corrosion-Driven Organic Coating Cathodic Delamination on Iron, Journal of the Electrochemical Society. 152 (2005) B73-B85. https://doi.org/10.1149/1.1850857

[59] A. Leng, A. H. Streckel, K. Hoffman, M. Stratmann, The delamination of polymeric coatings from steel Part 3: Effect of the oxygen partial pressure on the delamination reaction and current distribution at the metal/polymer interface, Corrosion Science. 41 (1998) 599-620. http://doi.org/10.1016/S0010-938X(98)00168-1.

[60] A. P. Nazarov, D. Thierry, Studies in the electrical double layer at metal/polymer interfaces by scanning capacitive probe, Protection of Metals. 39 (2003) 55-62. https://doi.org/ 10.1023/A:1021995208966.

[61] G. Williams, H.N. McMurray, M.J. Loveridge. Inhibition of Corrosion-Driven Organic Coating Disbondment on Galvanised Steel by Smart Release Group II and Zn(II)-Exchanged Bentonite Pigments. Electrochim. Acta, 55 (2010) 1740-1748.

[62] G. Williams, S. Geary, H. N. McMurray, Smart release corrosion inhibitor pigments based on organic ion-exchange resins. Corrosion Science. 57 (2012) 139-147. https://doi.org/10.1016/j.corsci.2011.12.024

[63] C. F. Baes, R. E. Mesmer, The Hydrolysis of Cations, Wiley, New York (1976).

[64] Y. K. C. Duong-Ly, S. B. Gabelli, Chapter Seven - Salting out of Proteins Using Ammonium Sulfate Precipitation, Methods in Enzymology, Academic Press, 541, p. 85-94, (2014). https://doi.org/10.1016/B978-0-12-420119-4.00007-0.

[65] M. Pourbaix. Atlas of Electrochemical Equilibria in Aqueous Solutions, Pergamon Press, London (1974) p. 409.

[66] https://comptox.epa.gov/dashboard/dsstoxdb/results?search=DTXSID6020147#properties . Last accessed 7 April 2020

[67] A. Kokalj, Ab initio modelling of the bonding of benzotriazole corrosion inhibitor to reduced and oxidized copper surfaces, Faraday Discussion. 180 (2015) 415-438. https://doi.org/10.1039/C4FD00257A.

[68] N.K. Allam, A.A. Nazeer, E.A. Ashour, A review of the effects of benzotriazole on the corrosion of copper and copper alloys in clean and polluted environments, J. Appl. Electrochem., 39 (2009) 961-969. https://doi.org/10.1007/s10800-009-9779-4.

[69] A. Frigani, M. Fonsati, C. Monticelli, G. Brunoro, Influence of the alkyl chain on the protective effects of 1,2,3-benzotriazole towards copper corrosion: part I : inhibition of the anodic and cathodic reactions, Corrosion Science. 41(1999)1205–1215. https://doi.org/10.1016/S0010-938X(98)00191-7.

[70] S. Mamas, T.Kıyak, M. Kabasakaloglu, A. Koc, The effect of benzotriazole on brass corrosion, Mater.Chem.Phys. 93(2005) 41–47. https://doi.org/10.1016/j.matchemphys.2005.02.012.

[71] J.Rodriguez, M. Mouanga, A. Roobroeck, D. Cossement, A. Mirisola, M.-G. Olivier, Study of the inhibition ability of benzotriazole on the Zn-Mg coated steel corrosion in chloride electrolyte, Corrosion Science.132 (2018) 56–67. https://doi.org/10.1016/j.corsci.2017.12.025.

[72] J. B. Cotton, The control of surface reactions on copper by means of organic reagents, Proceedings of the 2nd Inter. Congress on Metallic Corrosion (1963) 590–596.

[73] R. Youda, H. Nishihara, K. Aramaki, SERS and impedance study of the equilibrium between complex formation and adsorption of benzotriazole and 4-hydroxybenzotriazole on a copper electrode in sulphate solutions, Electrochim. Acta 35 (6) (1990) 1011–1017. https://doi.org/10.1016/0013-4686(90)90036-Y.

[74] E. Kondoh, T. Kawakami, M. Watanabe, L. Jin, S. Hamada, S. Shima, H. Hiyama, Structures of Cu surfaces developing in benzotriazole solutions: effect of pH, Jpn. J. Appl.Phys.5 6(2017)07KH01. https://doi.org/10.7567/JJAP.56.07KH01.

Figure 1. The BTA percentage release from ZnPhos-BTA in distilled water and 0.86 mol.dm^{-3} NaCl of varying pH.
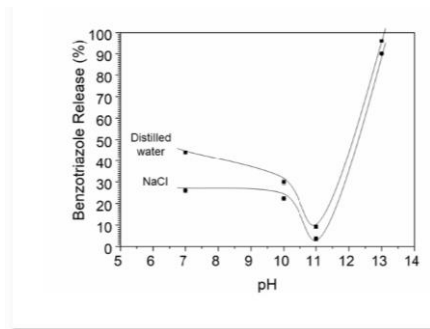
Figure 2. SKP derived E_{corr} as a function of distance from defect (x_{del}) profiles for the delamination of a PVB model coating, from a HDG substrate after initiation using a 0.86 mol.dm^{-3} NaCl electrolyte. t_i= 270 minutes.
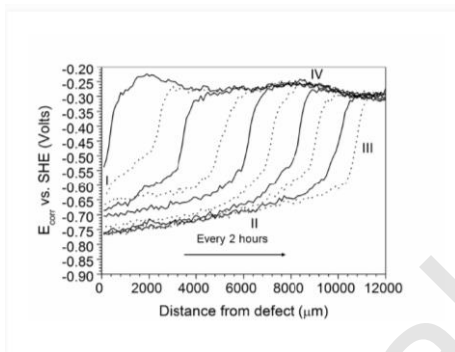

Figure 3. SKP derived E_{corr} as a function of distance from defect (x_{del}) profiles for the delamination of a PVB model coating pigmented with a.) 0.05 ϕ ZnPhos, b.) 0.1 ϕ ZnPhos and c.) 0.2 ϕ ZnPhos from a HDG substrate after initiation using a 0.86 mol.dm^{-3} NaCl electrolyte.
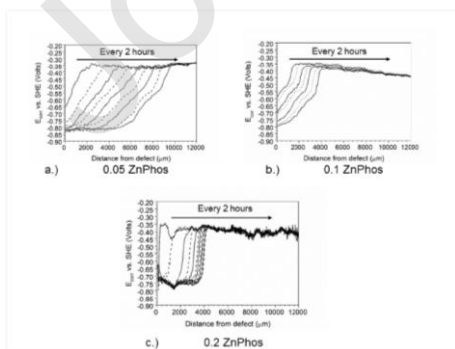
Figure 4. Distance that an unpigmented and ZnPhos pigmented PVB coating have delaminated from the defect (x_{del}) as a function of time, as derived from SKP data shown in Figure 3.
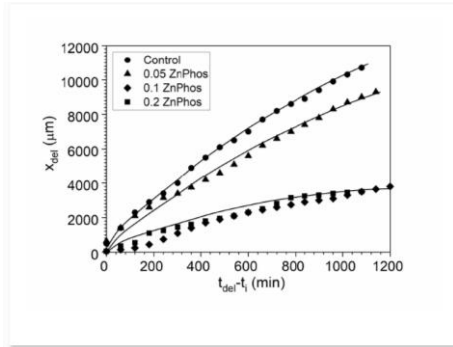

Figure 5. SKP derived E_{corr} as a function of distance from defect (x_{del}) profiles for the delamination of a PVB model coating pigmented with a.) 0.01 ϕ ZnPhos-BTA, b.) 0.05 ϕ ZnPhos-BTA and c.) 0.1 ϕZnPhos-BTA from a HDG substrate after initiation using a 0.86 M NaCl electrolyte.
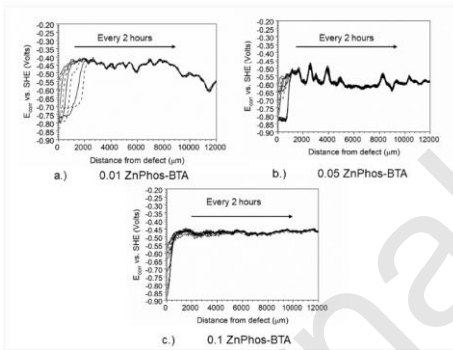

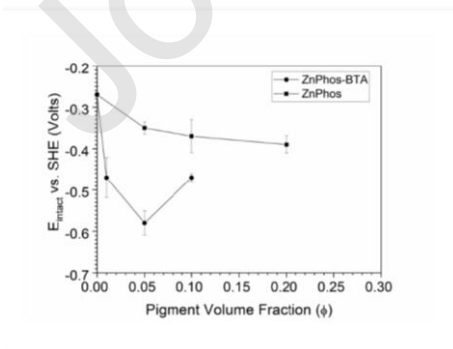Figure 6. E_{intact} of PVB coated HDG as a function of ZnPhos and ZnPhos-BTA ϕ.

Figure 7. Distance that an unpigmented and ZnPhos-BTA pigmented PVB coating have delaminated from the defect (x_{del}) as a function of time, as derived from SKP data shown in Figure 5.
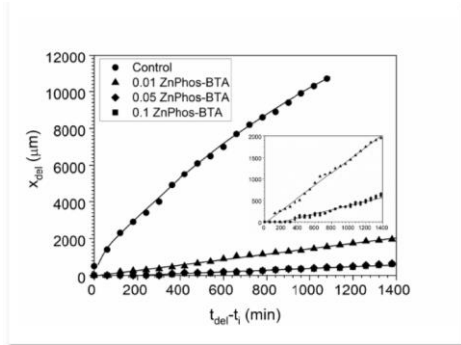

Figure 8. Cathodic delamination rate constant (k_{del}) as function of ZnPhos and ZnPhos-BTA and strontium chromate [48].
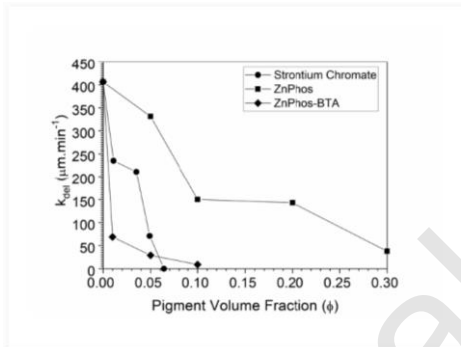

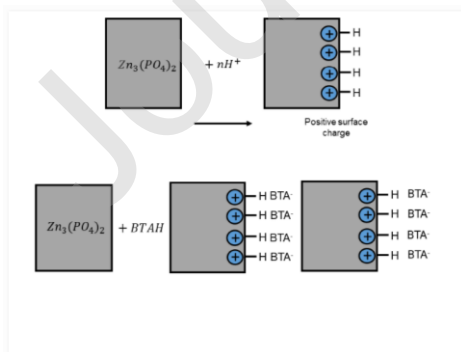Figure 9. Schematic of the mechanism by which BTA may adsorb onto a ZnPhos surface.

Figure 10. Schematic showing the pH dependent release of BTA from ZnPhos-BTA.

Increased Solubility of BTAH	Minimum Solubility	Increased Solubility
pH <8	pH 9-11	pH >11

$$Zn^{2+} + 2BTAH \rightleftharpoons Zn(BTA)_2 \rightleftharpoons Zn(OH)_4^{2-} + 2BTA$$

$+2H^+$ $+4OH^-$
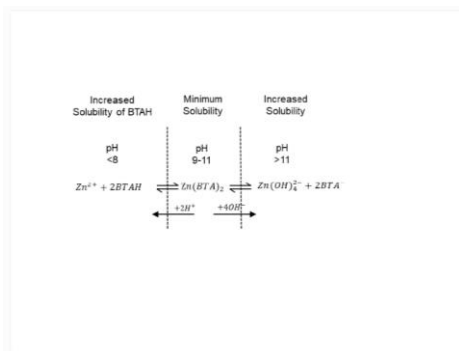
Tables

Table 1. The concentration of BTA released from ZnPhos-BTA in distilled water (1 g.dm^{-3}) and 0.86 mol.dm^{-3} NaCl of varying pH

Release Environment	BTA Concentration (M)	Release Percentage (%)
pH 7 distilled water	3.8×10^{-4} ($\pm 3 \times 10^{-6}$)	44.0 ± 0.5
pH 7 NaCl	2.2×10^{-4} ($\pm 5 \times 10^{-6}$)	26.0 ± 0.9
pH 10 distilled water	2.5×10^{-4} ($\pm 1 \times 10^{-5}$)	30.0 ± 1.4
pH 10 NaCl	1.9×10^{-4} ($\pm 6 \times 10^{-6}$)	22.3 ± 0.9
pH 11 distilled water	7.7×10^{-5} ($\pm 8 \times 10^{-6}$)	9.2 ± 0.9
pH 11 NaCl	3.0×10^{-5} ($\pm 9 \times 10^{-6}$)	3.6 ± 1.0
pH 13 distilled water	8.0×10^{-4} ($\pm 6 \times 10^{-6}$)	95.9 ± 0.6
pH 13 NaCl	7.6×10^{-4} ($\pm 8 \times 10^{-9}$)	89.9 ± 0.6

Table 2. Values of the cathodic delamination rate constant (k_{del}), inhibition efficiency, delamination initiation time (t_i) and intact potential (E_{intact}) obtained for the delamination of PVB, pigmnted with varying ϕ of ZnPhos, from a HDG substrate.

ZnP (ϕ)	k_{del} (µm min^{-1})	k_{del} reduction (%)	t_i (min)	E_{intact} vs. SHE (Volts)
0	9.3 ± 0.24		0	-0.27 ± 0.020
0.05	7.4 ± 0.11	20	60	-0.35 ± 0.015
0.1	3.2 ± 0.10	66	420	-0.37 ± 0.040
0.2	3.3 ± 0.12	65	180	-0.39 ± 0.021

Table 3. Values of cathodic delamination rate constant (k_{del}), inhibition efficiency, delamination initiation time (t_i) and intact potential (E_{intact}) obtained for the delamination of PVB, pigmnted with varying ϕ of ZnPhos-BTA, from a HDG substrate.

ZnP-BTA (ϕ)	k_{del} (µm min^{-1})	k_{del} reduction (%)	t_i (min)	E_{intact} vs. SHE (Volts)
0	9.3±0.24		0	-0.27±0.020
0.01	1.5±0.02	84	540	-0.47±0.048
0.05	0.5±0.02	95	480	-0.58±0.029
0.1	0.5±0.02	95	2100	-0.47±0.009

Table 4. The calculated K_{sp} values for the Zn(BTA)$_2$ complex at varying pH.

pH	K_{sp} (mol^3.dm^{-9})
7	2.7×10^{-11}
10	7.9×10^{-12}
11	2.2×10^{-13}
13	2.6×10^{-10}